ELSEVIER

Journal of Power Sources 73 (1998) 23–29

JOURNAL OF POWER SOURCES

Structure and properties of lead–calcium–tin alloys for battery grids

C.S. Lakshmi [a,*], J.E. Manders [b], D.M. Rice [b]

[a] *Pasminco Ltd., PO Box 175, Boolaroo, NSW 2284, Australia*
[b] *Pasminco Ltd., PO Box 129K, Melbourne, VIC 3001, Australia*

Received 23 September 1997; accepted 10 October 1997

Abstract

The selection of an appropriate alloy composition for battery grids is essential for the performance and long life of lead/acid batteries. This investigation examines the effects of the variation of calcium (0.03 to 0.13 wt.%) and tin (0.3 to 1.5 wt.%) content on the microstructure, mechanical properties and the corrosion resistance of cast Pb–Ca–Sn battery grids. Both corrosion resistance and the mechanical properties are found to increase with increasing tin and decreasing calcium levels. The relationship between the alloy composition and the resulting properties of the grids is discussed.

Keywords: Lead–calcium–tin; Grid alloys; Microstructure; Corrosion; Lead/acid batteries

1. Introduction

In recent years, the use of lead–calcium–tin alloys has become more common for producing lead/acid battery grids. In particular, lead–calcium–tin grids are being employed for both the positive and the negative grids of valve-regulated lead/acid (VRLA) batteries. Hence, in view of the growing demand for VRLA batteries, recent investigations of the Pasminco–CSIRO research program we have focused on the effects of various elemental additions to lead–calcium grid alloys.

The selection of appropriate levels of elements for the battery grids involves considerations of grid-production capability, economic feasibility, and the metallurgical and electrochemical properties of the resulting alloys. As the properties of grids are highly dependant on the amount of each alloying element present, the effects of alloying additions have been studied for a whole range of alloy compositions viz., calcium 0.03 to 0.13 wt.%, tin 0.3 to 1.5 wt.%. The work reported here deals with the first phase of the investigation and is based on alloys that contain a maximum bismuth content of 0.005 wt.%. In particular, a systematic study has been made of the effects of calcium and tin on the mechanical properties and corrosion behaviour of the cast grids as dictated by the structure of the alloy.

* Corresponding author.

2. Experimental procedure

2.1. Alloy composition

Lead–calcium–tin grids with varying calcium and tin content were cast using a Wirtz 40C grid caster. In order to maintain the level of calcium constant throughout the casting run of a specific alloy, the lead–calcium–tin alloys contained aluminium in the range 0.015–0.025 wt.%. The grids were air-cooled after casting. The compositions of the grid alloys under test can be grouped into: (i) high-calcium alloys; (ii) low-calcium alloys. It should be noted that the compositions quoted in this paper are in wt.%, unless stated otherwise.

2.1.1. High-calcium alloys

The high-calcium alloys have a calcium content in the range 0.09–0.13 wt.%, and a tin level in the range 0.3 to 1.0 wt.%. The average compositions of the cast grids as measured by inductively coupled plasma spectroscopy are given in Table 1. This analysis was conducted on samples taken from both lugs and grid wires.

2.1.2. Low-calcium alloys

The low calcium-alloys are listed in Table 2. At a calcium level of 0.06 wt.%, the tin content was varied from 0.3 to 1.5 wt.%. At 0.03 wt.% calcium, an alloy with 0.6 wt.% tin was studied.

Table 1
Compositions of high-calcium alloy grids (wt.%)[a]

Alloy	Calcium	Tin	Aluminium	Tin-to-calcium ratio r
1	0.13	0.3	0.014	2.31
2	0.11	0.3	0.015	2.72
3	0.09	0.3	0.011	3.33
4	0.13	0.6	0.011	4.62
5	0.11	0.6	0.014	5.45
6	0.09	0.6	0.013	6.67
7	0.13	1.0	0.019	7.69
8	0.11	1.0	0.012	9.09
9	0.09	1.0	0.012	11.11

[a]Average of three grids-cast at the beginning, middle, and end of the casting run.

2.2. Microstructure

Cast grids of various compositions were stored at room temperature and the microstructures of grids after one week were examined using an Olympus PMG3 optical microscope. The metallographic samples were prepared by mounting the lugs, as well as the grid wires, in Struers Epofix at room temperature. The ground samples were chemically polished using a 3:1 (by volume) acetic acid: (30%) hydrogen peroxide solution, followed by a wipe etch with a solution containing 7 g ammonium molybdate and 15 g citric acid.

2.3. Mechanical properties

Rectangular (flat) tensile specimens with a length of 90 mm, a width of 10 mm and a thickness of 1.5 mm were cast (mould temperature = 160°C) using the molten alloy from the melt pot of the grid caster. Four specimens were tested for each alloy composition. The ultimate tensile strength and elongation were noted for each specimen. Tensile tests were carried out on cast samples of high-calcium alloys after storage at room temperature for one week.

The plain end of each cast tensile sample was used for conducting hardness measurements. These measurements were made over a period of about 80 days using a DVK-2 hardness tester in the Brinell mode. For each alloy composition, three readings were taken on two different samples.

Table 2
Compositions of low-calcium alloy grids (wt.%)[a]

Alloy	Calcium	Tin	Aluminium	Tin-to-calcium ratio r
10	0.06	0.3	0.013	5
11	0.06	0.6	0.019	10
12	0.06	0.8	0.017	13.33
13	0.06	1.0	0.020	16.67
14	0.06	1.5	0.016	25
15	0.03	0.6	0.020	20

[a]Average of three grids—cast at the beginning, middle, and end of the casting run.

The average value was then used for plotting graphs of hardness versus ageing time. The Brinell hardness (HB) numbers were computed using the following formula:

$$\mathrm{HB} = 2P/\left\{3.1416\,D\left[D-\sqrt{(D^2-d^2)}\right]\right\} \quad (1)$$

where P = applied load (kgf); D = diameter of the indentor ball (mm); d = diameter of the impression (mm).

2.4. Bare-grid corrosion tests

The corrosion behaviour of bare grids was determined under constant-current conditions. A constant current of 0.5 A/grid was passed through sets (cells) of positive and negative grids connected in series, with the electrolyte (sulfuric acid with a specific gravity of 1.275) temperature maintained at 40°C; each cell comprised 5 positives and 6 negatives. The initial weight of each positive grid was taken prior to assembly in the cell. Separate cells were assembled using grids of the same composition.

Two corrosion experiments were performed for each alloy composition over a maximum period of 27 days. Individual grids were removed periodically (every 4 to 6 days) from each cell. The corrosion product from each corroded grid was dissolved in a boiling solution of sodium hydroxide (100 g l^{-1}), mannitol (20 g l^{-1}) and hydrazine (4 g l^{-1}). The cleaned grids were thoroughly rinsed with water, dried and weighed. The corrosion rates of the grids were compared in terms of the weight loss. The morphology of grids cleaned after 27 days of testing was also examined.

3. Results and discussion

3.1. Microstructure

Typical microstructures of high-calcium alloy grids (aged at room temperature for one week), as observed in the central regions of the lugs are shown, in Figs. 1 and 2. It is clear that the variation in composition significantly changes the grain structure of the alloy. In general, the grain size increases with increasing tin content (Fig. 1) but decreases with calcium content (Fig. 2). It is also seen that the grain boundaries are not regular, but are serrated, which is characteristic of lead–calcium alloys.

The microstructures of low-calcium alloys (Pb–0.06 wt.% Ca–Sn) with varying tin contents (from 0.3 to 1.0 wt.%), as observed in the central part of the lug and the grid wire, are given in Fig. 3. The microstructures clearly show an increase in the grain size with increasing tin content. Furthermore, the grain boundaries are serrated at low tin concentrations and become smooth as the tin content increases. It is interesting to note that at tin contents of 0.8 wt.% and above, the grain size becomes so large that there are only two to three grains across the

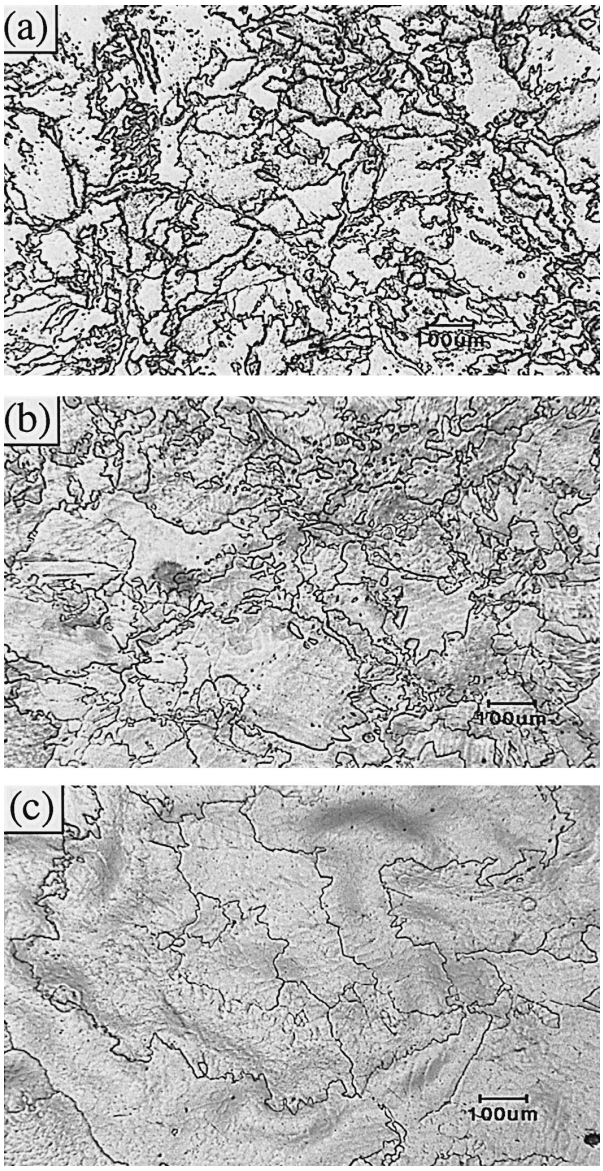

Fig. 1. Effect of tin on microstructure of high-calcium alloys: (a) Pb–0.11 wt.% Ca–0.3 wt.% Sn; (b) Pb–0.11 wt.% Ca–0.6 wt.% Sn; (c) Pb–0.11 wt.% Ca–1.0 wt.% Sn.

width of the grid wire. The effect of calcium addition to Pb–0.6 wt.% Sn alloy is demonstrated in Fig. 4. As with high-calcium alloys, the grain size increases with decreasing calcium level.

The microstructures shown in Figs. 1–4 indicate that in the case of both high- and low-calcium alloys, the grain size and morphology vary significantly with calcium and tin content in the alloy. In previous studies [1,2], the lead–calcium–tin alloys have been characterized by the tin-to-calcium ratio (r). The microstructure is found to differ at a critical value of about $r = 9$.

In this investigation, it has been observed that for r values less than 9 (Fig. 1a,bFig. 2) the grains are smaller in size (30 to 200 μm) and the grain boundaries are serrated, as observed in binary lead–calcium alloys. In binary lead–calcium and ternary lead–calcium–tin systems, this serrated structure has been explained in terms of the cellular precipitation of Pb_3Ca behind the moving grain boundaries [3–5] during solidification.

When the r value exceeds 9 (Fig. 1cFig. 3c), the grains are well-defined and larger in size (150 to 100 μm) with a cellular substructure of segregated tin. According to Bouirden et al. [1] and others [3,6], at high values of r, tin is segregated in intercellular regions and the calcium precipitation is converted from cellular to continuous precipitation to form more stable $(Pb,Sn)_3Ca$. This is followed by several discontinuous transformations to form Sn_3Ca precipitates [7].

According to Hertz et al. [8], the solid solubility of calcium is decreased by the addition of tin. Hence, irre-

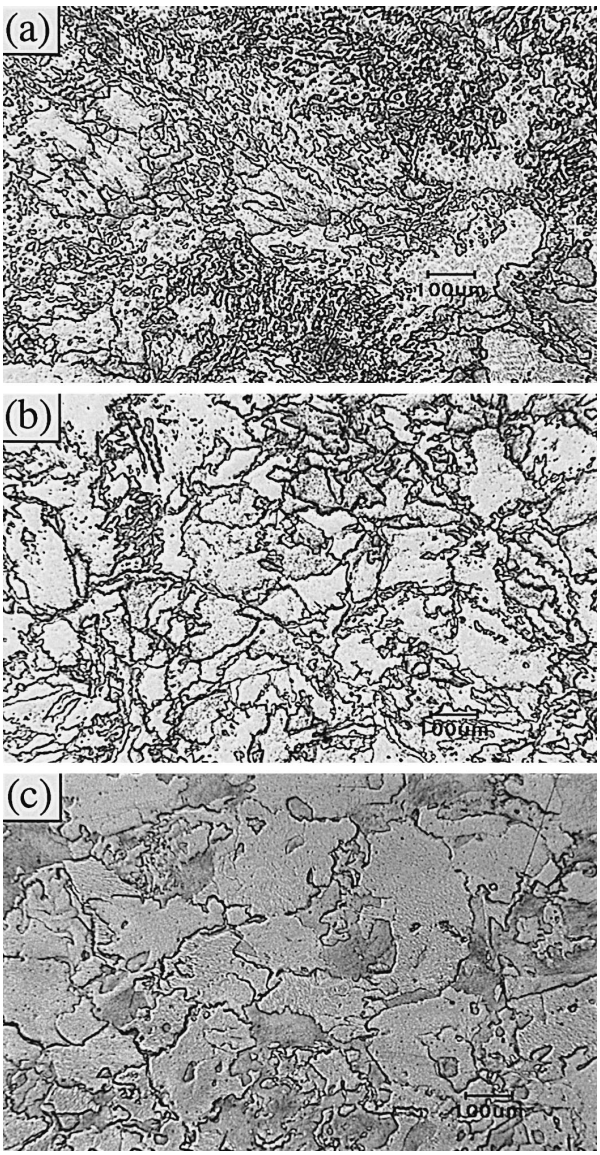

Fig. 2. Effect of calcium on microstructure of high-calcium alloys: (a) Pb–0.13 wt.% Ca–0.3 wt.% Sn; (b) Pb–0.11 wt.% Ca–0.3 wt.% Sn; (c) Pb–0.09 wt.% Ca–0.3 wt.% Sn.

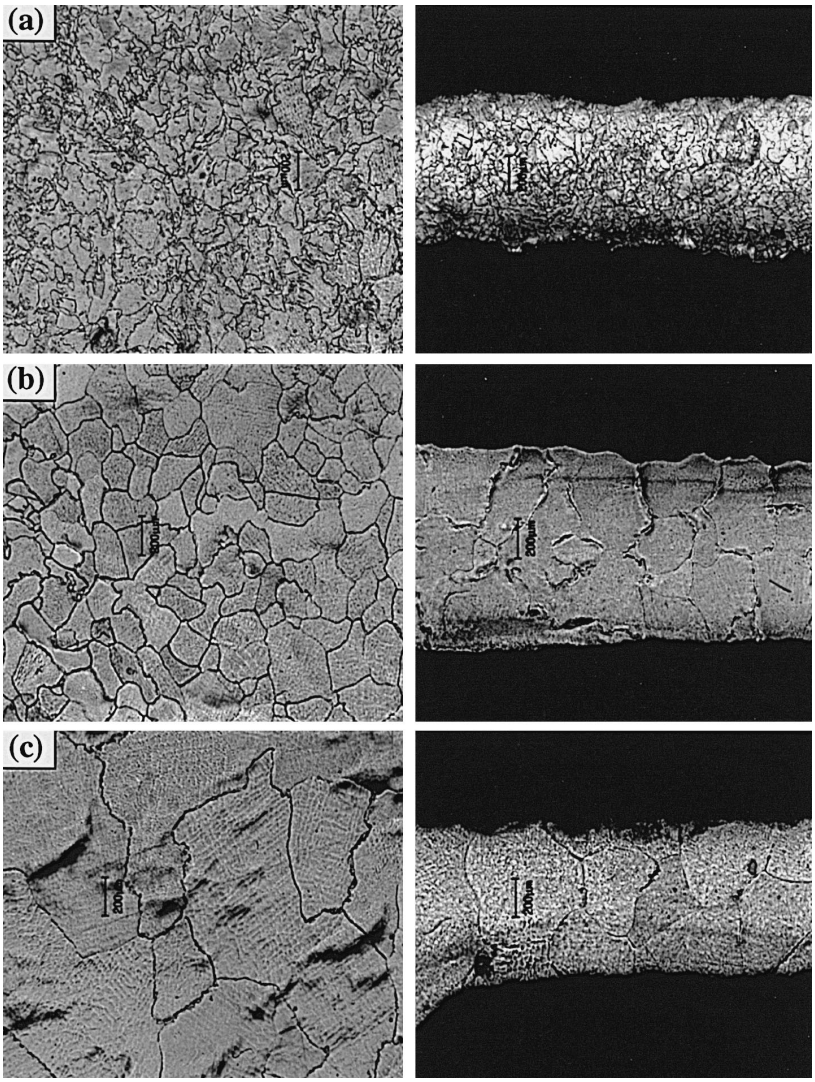

Fig. 3. Micrographs of low-calcium alloys with increasing tin concentration. Left: Lug regions, Right: Grid wires; (a) Pb–0.06 wt.% Ca–0.3 wt.% Sn, (b) Pb–0.06 wt.% Ca–0.6 wt.% Sn, (c) Pb–0.06 wt.% Ca–1.0 wt.% Sn.

spective of the r value, when the calcium level is above 0.08 wt.% the excess of insoluble calcium forms precipitates and a fine grain structure is expected. In this investigation, however, large grains are observed even for alloys with >0.08 wt.% Ca, as shown in Fig. 1c for a Pb–0.11 wt.% Ca–1.0 wt.% Sn alloy. Nevertheless, the r value appears to determine the grain size and the resulting properties, as discussed below.

3.2. Mechanical properties

3.2.1. Age hardening

The age-hardening behaviour of various high-calcium alloys as a function of calcium and tin content over a period of 3 months is shown in Figs. 5 and 6, respectively. At a calcium level of 0.09 wt.% (Fig. 5a), the rate of hardening as well as the peak hardness increases with increasing tin content. The same trend is seen with alloys containing 0.11 wt.% Ca (Fig. 5b) and 0.13 wt.% Ca (Fig. 5c). It is also seen that at a constant tin level (Fig. 6), the hardness of the alloy increases with decreasing calcium content. It shows he noted, however, that as there is little variation in the calcium content, the change in hardness is negligible.

The age-hardening behaviour of some low-calcium alloys is shown in Fig. 7 and the results are consistent with previous studies [1,9]. Again, peak hardness increases with increasing tin concentration. These results suggest that there is a distinct difference between the age-hardening behaviour of high- and low-calcium alloys.

The age-hardening behaviour of lead–calcium and lead–calcium–tin alloys has been studied extensively by several researchers [1,9–11]. In agreement with these investigations, the results of this study also suggest that the age-hardening of Pb–Ca–Sn alloys is determined by the ratio of tin-to-calcium concentration, r, in the alloy.

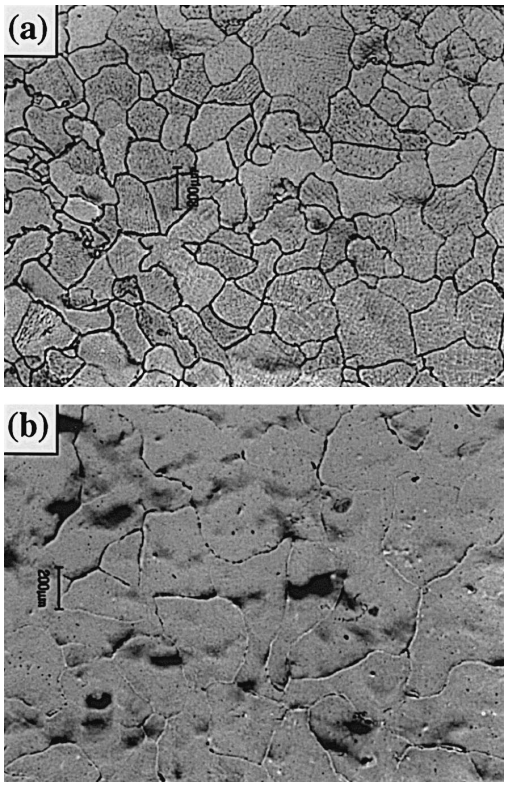

Fig. 4. Effect of calcium on the microstructure: (a) Pb–0.06 wt.% Ca–0.06 wt.% Sn and (b) Pb–0.03 wt.% Ca–0.6 wt.% Sn.

Typical, initial, age-hardening behaviour of both high- and low-calcium alloys for various r values is shown in Fig. 8. For high-calcium alloys with $r < 9$, the hardening occurs very quickly and reaches a hardness value of 12 to 14 HB within a day. After the initial period, the alloys continue to harden at a decreasing rate. In contrast, a low-calcium alloy with $r > 9$ exhibits a very low initial hardness ($\sim$7 HB) and hardens at a considerably slower rate for up to 6 days after casting. This initial slow rate is followed by a rapid rate of hardening.

The mechanisms of age hardening in lead–calcium–tin alloys have been explained [1,10,11] in terms of structural transformations/reactions that result in the formation of precipitates such as Pb_3Ca, $(PbSn)_3Ca$ and Sn_3Ca. For low r values, Pb_3Ca precipitates are formed and are believed to impart rapid initial hardness. For high r values, more stable effective $(PbSn)_3Ca$ and Sn_3Ca precipitates are considered to harden the lead matrix; but as the formation of these precipitates occurs at a very slow rate, the initial hardness is delayed for high tin alloys.

3.2.2. Tensile properties

The ultimate tensile strength (UTS) for the various alloy samples measured one week after casting is presented in Fig. 9. The error bars shown in this plot represent a '95% confidence interval' and the small solid squares each represent the mean of four measurements. At all calcium levels, the UTS values of the alloys increase with increasing tin content. Similar results have been reported by Prengaman [3] for both cast and wrought lead–calcium–tin alloys. The improvement in the mechanical strength is again due to the change in precipitation mode from Pb_3Ca to $(PbSn)_3Ca$ with increasing tin level.

3.3. Corrosion behaviour

The results from constant-current bare grid corrosion tests on high-calcium alloys are given in Fig. 10. These plots of weight loss as a function of exposure time show that the corrosion rate decreases with increasing tin content or decreasing calcium content. The Pb–0.13 wt.% Ca–0.35 wt.% Sn alloy exhibits the highest corrosion rate and the Pb–0.09 wt.% Ca–1.0 wt.% Sn alloy the lowest corrosion rate.

The corresponding corrosion behaviour of low-calcium alloys is presented in Fig. 11. For grids containing Pb–0.06 wt.% Ca. The rate of corrosion is decreased by $\sim$30% on raising the level of tin from 0.3% to 1.5 wt.%. The Pb–0.03 wt.% Ca–0.6 wt.% Sn alloy with the lowest calcium content displays the lowest rate of corrosion.

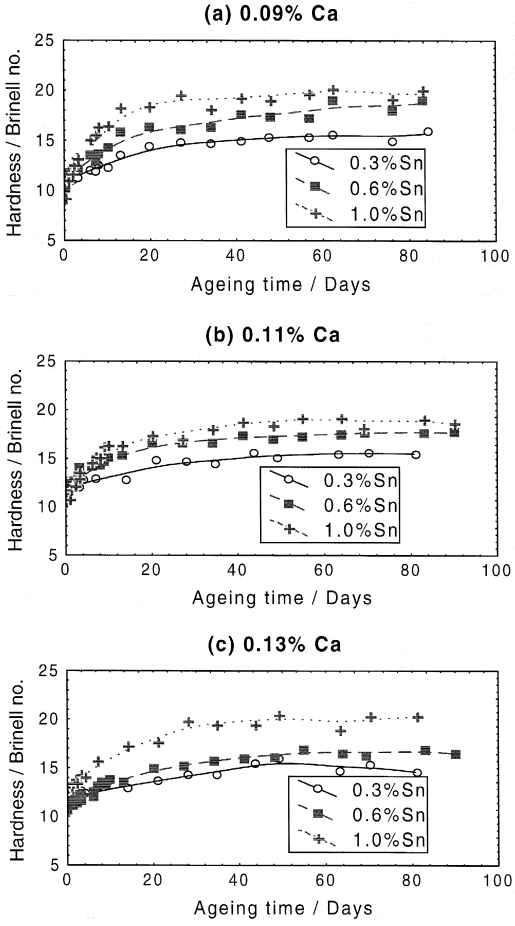

Fig. 5. Effect of tin on age-hardening behaviour of high-calcium alloys at various calcium levels.

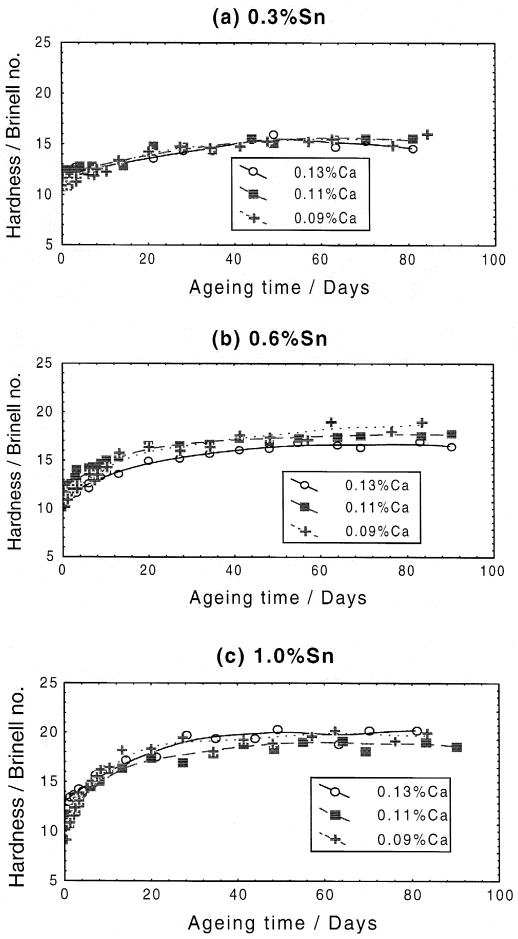

Fig. 6. Effect of calcium on age-hardening behaviour of high-calcium alloys at various tin levels.

Combining the results of high- and low-calcium alloys (Fig. 12), it is seen that, at a tin level of 0.6 wt.%, the weight loss after 30 days is decreased by about 43% by reducing the level of calcium from 0.13 to 0.03 wt.%.

In this study, the casting conditions during the production of grids as well as the environmental conditions used for accelerated corrosion testing were held constant. Hence, the corrosion behaviour of the grids can be compared directly in terms of the microstructure, which is mainly

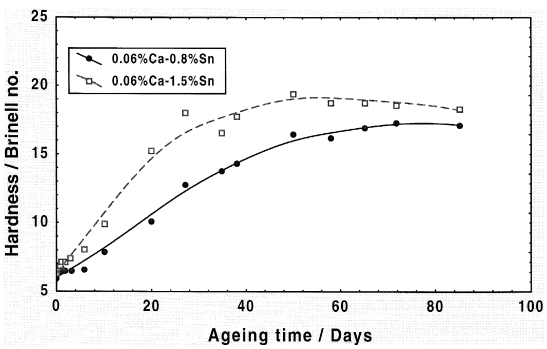

Fig. 7. Age-hardening behaviour of low-calcium alloys.

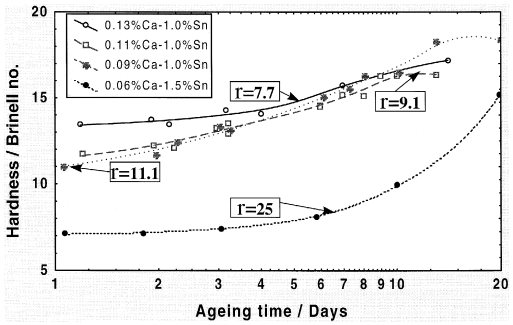

Fig. 8. Initial age-hardening behaviour of high- and low-calcium alloys.

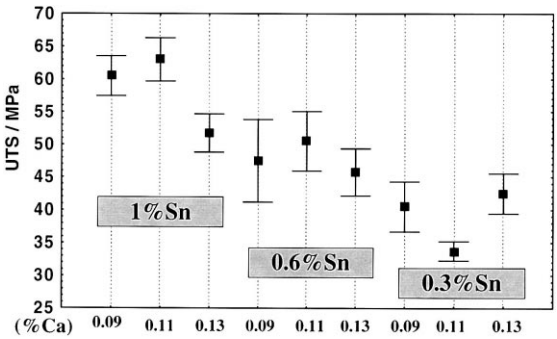

Fig. 9. Tensile properties of high-calcium alloys.

dependent on the alloy composition. In general, alloys with a fine grain structure have extensive grain boundary areas and hence will exhibit more weight loss due to corrosion.

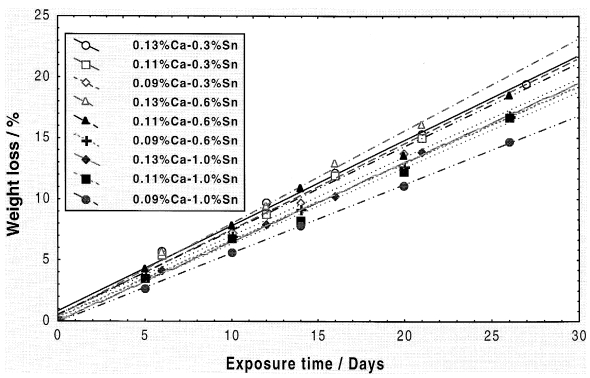

Fig. 10. Corrosion behaviour of high-calcium alloys.

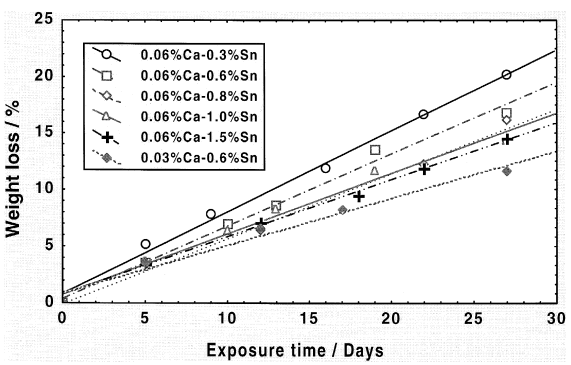

Fig. 11. Corrosion behaviour of low-calcium alloys.

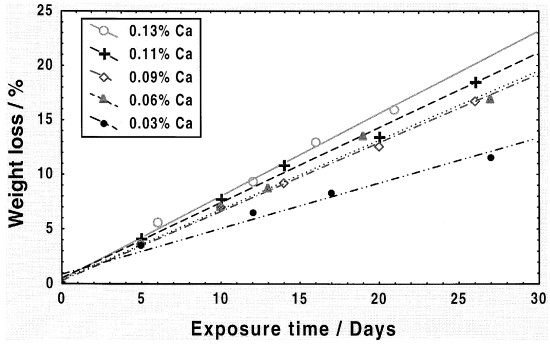

Fig. 12. Corrosion behaviour of high- and low-calcium alloys with a tin content of 0.6 wt%.

By contrast, alloys with coarse grains will suffer less weight loss and attack from and deep intergranular corrosion will be more prevalent.

The weight-loss data shown in Figs. 10–12 indicate that the corrosion resistance of Pb–Ca–Sn alloys increases significantly with increasing tin and decreasing calcium content. This is in agreement with the microstructural observation that the grain size increases with increasing levels of tin and decreasing levels of calcium. For Pb–0.07 wt.% Ca–y wt.% Sn ($y = 0.7$ to 2 wt.%) alloys, Giess and Ohlin [12] have also observed that the corrosion resistance increases at high levels of tin.

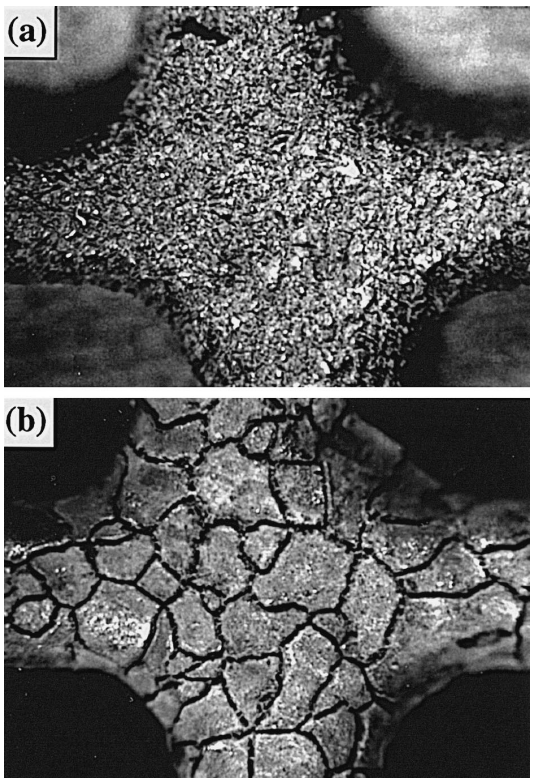

Fig. 13. Morphology of corroded grids: (a) Pb–0.06 wt.% Ca–0.3 wt.% Sn; (b) Pb–0.06 wt.% Ca–1.0 wt.% Sn.

3.4. Corrosion morphology

The typical morphology of corroded grids after the removal of corrosion products is shown in Fig. 13. The extent of corrosion is determined by the nature of the surface morphology. For alloys with small grain boundaries and higher weight loss, the surface morphology is very rough (Fig. 13a). This is due to uniform corrosion throughout the surface. On the other hand, for alloys with large grains, the surface of the corroded grids is smooth (Fig. 13b) and corrosion occurs preferentially along the grain boundaries. As noted earlier, at high tin levels (0.8 wt.% and above) the number of grains across a grid wire can be as low as two and thus although the total weight loss is low, the grids are susceptible to penetrating corrosion and this may lead to catastrophic failure.

4. Conclusions

(i) The properties of lead–calcium–tin alloys depend mainly on the ratio of tin content to calcium content.

(ii) Alloys with low tin-to-calcium ratios (< 9) exhibit fine grain size, rapid age hardening, and high corrosion rates.

(iii) Alloys with high tin-to-calcium ratios (> 9) exhibit large grain size, slow initial age hardening, and low corrosion rates. Due to intergranular penetrating type of corrosion, however, catastrophic failure of the grids may occur.

(iv) The corrosion resistance and mechanical properties of lead–calcium–tin alloys increase with increasing in and decreasing calcium levels.

References

[1] L. Bouirden, J.P. Hilger, J. Hertz, J. Power Sources 33 (1991) 27.
[2] R.D. Prengaman, J. Power Sources 53 (1995) 207.
[3] R.D. Prengaman, J. Power Sources 33 (1991) 13.
[4] H. Borchers, W. Scharfenberger, S. Henkel, Z. Metallkd. 64 (1973) 478.
[5] R.D. Prengaman, Spring Meeting, Electrochemical Society, Chicago, IL, Paper 217, May 1973.
[6] J. Hertz, C. Fornasieri, J.P. Hilger, M. Notin, Proceedings of Labat 93, Varna, Bulgaria, 1993, p. 42.
[7] R.D. Prengaman, Mater. Sci. Technol. 8 (1996) 71.
[8] J. Hertz, C. Fornasieri, J.P. Hilger, M. Notin, J. Power Sources 46 (1993) 299.
[9] H.K.G. Assmann, Patent No. 27 58 940 (5 July 1979).
[10] J.P. Hilger, L. Bouirden, J. Alloys Compounds 236 (1996) 224.
[11] H. Tsubakino, R. Nozato, A. Yamamoto, Z. Metallkd. 84 (1993) 29.
[12] H. Giess, C. Ohlin, Intelec 96, 1996, p. 334